TELKOMNIKA Telecommunication Computing Electronics and Control
Vol. 24, No. 1, February 2026, pp. 313~328
ISSN: 1693-6930, DOI: 10.12928/TELKOMNIKA.v24i1.27276

Optimizing planar micro-transformer performance

Tahar Alili[1], Fatima Zohra Medjaoui[1], Azzedine Hamid[1,2], Abderrahim Mokhefi[3], Yacine Guettaf[2], Hocine Guentri[2]
[1]Department of Electrotechnics, Faculty of Electrical Engineering, University of Science and Technology of Oran USTO-MB, Oran, Algeria
[2]Department of Electrical Engineering, Institute of Technology, Nour El Bachir University Center, El Bayadh, Algeria
[3]Institute of Mechanical Engineering, National Polytechnic School of Oran Maurice Audin, Oran, Algeria

Article Info

Article history:

Received Jun 12, 2025
Revised Nov 22, 2025
Accepted Dec 8, 2025

Keywords:

Converter flyback
Heat transfer
Magneto-thermal
Microcoils
Micro-converter
Micro-transformer
Thermal convection

ABSTRACT

Faced with new requirements for isolated switching power supplies with high efficiency and power density, planar transformer technology has emerged as a serious alternative to wound components. The work presented in this paper addresses the issue of developing planar transformers in the context of low-power electronics, where volume and weight constraints are paramount. The flat shape of the coils and the interlacing of the windings do not allow for control of magneto-thermal phenomena. Although scientific literature offers numerous simulation tools to aid in the design of such transformers, it must be noted that they do not allow for a rigorous account of these phenomena. In this paper, methods and a geometric and electrical sizing tool in planar technology are used for the design of flyback direct current to direct current (DC/DC) converters. Methods for dimensioning and estimating temperature rise are presented and compared in order to develop calculation tools for design purposes. This study enabled us to observe the distribution of the magnetic field, the role of ferrite, the distribution of currents and voltages in the coils, and the distribution of temperature in our device. It should be noted that conductive and convective heat transfer processes were considered in steady state.

Corresponding Author:

Hocine Guentri
Department of Electrical Engineering, Institute of Technology, Nour El Bachir University Center
BP 900, El Bayadh 32000, Algeria
Email: h.guentri@cu-elbayadh.dz

1. INTRODUCTION

Work on integrating passive magnetic components (inductors and transformers) has been growing significantly in recent years. The objectives of this work are to reduce component size in order to lower costs and to develop appropriate technological approaches for manufacturing these components. These components are generally used in the form of stacked conductive, insulating and magnetic layers. The targeted applications concern low-power electronics, inductance for direct current to direct current (DC-DC) converters [1] and planar transformers for isolated power switch control [2] ranging from a few kHz to a few GHz [3], [4]. However, there is limited research into the use of magnetic materials for the manufacture of integrated components [5].

Power electronics research in recent years has primarily focused on improving converter performance in terms of efficiency, compactness, and reliability, particularly transformers. Li *et al.* [6] presented a localised element model to represent the behaviour of millimetre wave (MW) integrated transformers. This model has a 2-π architecture and contains the equations for evaluating the values of its components. These formulas rely on the transformer's geometrical and technological properties. In the article

by Ouyang *et al.* [7], the most important factors for the design of a planar transformer, including winding losses, core losses, leakage inductance and parasitic capacitance, were studied individually. Mu *et al.* [8] studied the design of a high-power density transformer and inductance for a high frequency double active bridge (DAB) GaN charger.

The designed transformer has an efficiency greater than 99.2% while delivering 3.3 kW. Compared with the transformer and inductance used in the 50 kHz charger, the developed transformer's power density is 6.3 times higher. The detailed design procedure and loss analysis are discussed. Compromises between these factors were analysed in order to obtain optimal parameters. Orosz [9] presented a fast approximation method useful in the initial design as well as a more detailed analysis of inductors and transformers. Eighty percent of a low-power converter's footprint is occupied by passive components, which serve a variety of purposes, including filtering, energy transfer, galvanic isolation, impedance matching, and temporary electrical energy storage. Liu *et al*. [10] presented in his article the main directions of development and trends in the design of power transformers.

The main research directions considered and future trends in the field of optimisation methods for preliminary design transformers are summarised. Liu *et al.* [11] proposed in their article the study of an isolated inductor–inductor–capacitor (LLC) resonant converter with a switching frequency in the MHz range in which conventional silicon devices are replaced by wide bandgap gallium nitride devices to reduce switching losses in the power device. Liu *et al.* [11] presented an optimisation design methodology aimed at minimising the size of the transformer core and improving converter performance through optimised winding configurations. The objective of this work is to study the magnetothermal behaviour of a microtransformer with a view to its integration into a flyback-type microconverter designed for low power and high frequencies.

The transformer is flat in shape, with square flat spiral primary and secondary microcoils. The design of this type of microcoil is based on the specifications of the microconverter. Three points are essential for its design: the choice of materials used in its construction, and its geometric and electrical dimensions [12], [13]. The results of the dimensioning will be useful for designing the mathematical model and performing various simulations of magnetothermal behaviour. To ascertain the ideal distribution of current and electrical potential in the conductor and, as a result, to get a good distribution of field lines, the magnetic component entails visualizing the distribution of current density, magnetic field lines, and electrical potential. For the thermal part [14], [15], it is necessary to visualise the temperature distribution of the coil and substrate.

The novelty of this article lies in the study of magnetic behaviour, where we observed the effect of the gap on the distribution of field lines likely to disturb adjacent components, as well as the effect of temperature, where we also visualised the effect of the gap on the temporal evolution of temperature in the different layers of the component. Conductive and convective heat transfer processes were taken into account in steady state. It should be noted that convective phenomena have never been taken into account in this type of situation. The simulations were performed using computation solver (COMSOL) Multiphysics simulation software.

2. FLYBACK MICRO-CONVERTER PRESENTATION

The flyback converter [16], [17], Figure 1, has been chosen because the micro-transformer is made up of fewer parts and a single wrapped component, Figure 2, and of a single switch. Moreover, it is frequently used for low power applications (<100W). We opted for the specifications from which we define the specifications of the micro-converter which is the starting point for the sizing of the micro-transformer. Input voltage $V_e = 12\,V$, output voltage $V_s = 5V$, output power $P_s = 5W$, operating frequency $f = 100\,MHz$.

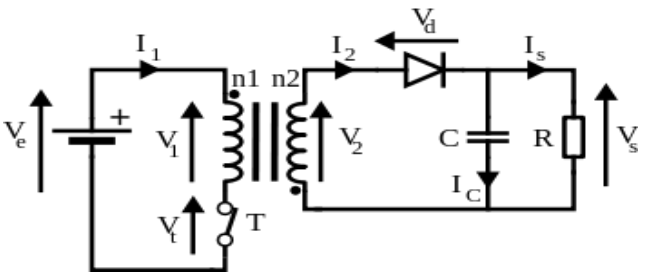

Figure 1. Electrical scheme of the flyback converter containing the micro transformer

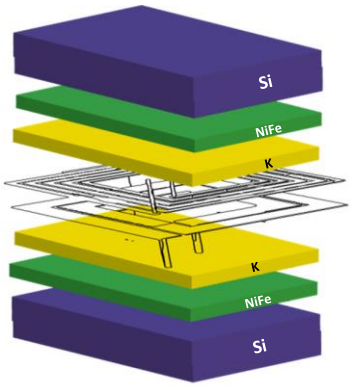

Figure 2. 3D model of the micro-transformer

2.1. Micro-transformer sizing

The volume of the magnetic core and the surface area where the electrical circuit of the micro-transformer will be installed are assessed, taking into account the specific electrical and magnetic properties of the micro-transformer. From this, the magnetic core's dimensions will be assessed while adhering to the micro-converter's requirements for magnetic energy storage and material losses [18], [19].

2.2. Geometrical parameters calculation

Square geometry microcoils are defined by a set of essential geometric parameters that directly influence their electromagnetic performance. The number of turns n determines the winding density and contributes to the increase in inductance. The width of the conductor w and its thickness t play a major role in the electrical resistance and heat dissipation capacity of the microcoil. Winding spacing affects both magnetic coupling and proximity losses. The total length of the conductor lt makes it possible to evaluate the overall ohmic resistance of the device. Finally, the outer diameter dout and inner diameter din characterize the physical size of the coil and influence the magnetic field produced at the center of the structure. The simultaneous optimization of these parameters is therefore essential to design efficient microcoils adapted to the targeted applications, such as microelectronics devices or integrated sensors, Figure 3.

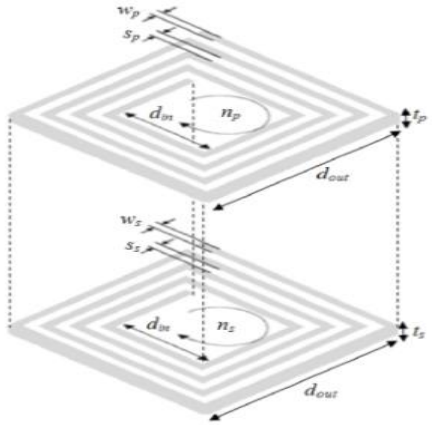

Figure 3. Micro-transformer primary and secondary coils geometrical parameters

2.3. Electrical parameters calculation

The equivalent electrical model, derived from the diagram presented in Figure 2, is used for the simulation of the electromagnetic behavior of the micro-transformer [18], [19] (see Figure 4). This model integrates all the electrical parameters representative of the device: the primary and secondary inductances Lp and Ls, associated respectively with the two windings; the series resistances Rsp and Rss, reflecting the ohmic losses; the $Coxp$ and $Coxs$ oxide capacities; the resistances of the magnetic layer $Rmagp$ and $Rmags$; as well as the resistances $Rsubp$ and $Rsubs$ and the capacitances $Csubp$, $Csubs$ associated with the

silicon substrate. Finally, the coupling capacitances Ckp and Cks specific to each winding, as well as the mutual capacitance Ck between the two windings, ensure the precise modeling of the electrostatic interactions internal to the micro-transformer.

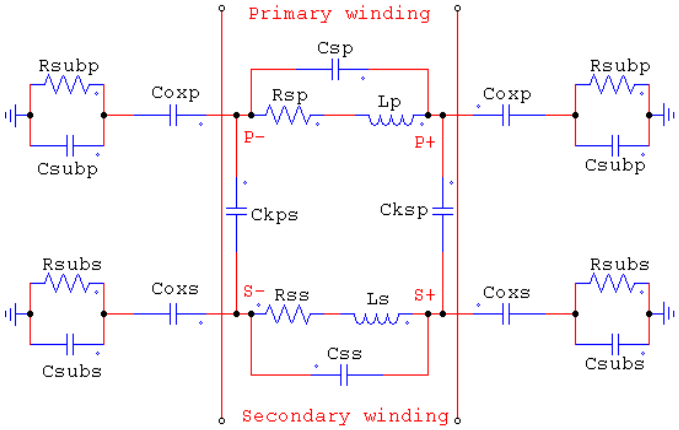

Figure 4. Equivalent electrical circuit of the micro-transformer

2.4. Magnetic circuit dimensioning

The transformation ratio m is one of the main electrical parameters of the micro-transformer, it is given by:

$$m == \frac{\propto V_{out}}{\propto -1 V_{in}} \tag{1}$$

The primary inductance L_p is calculated for a maximum current ripple: $\alpha = 0.5$

$$Lp = \frac{V_{in}^2 \propto^2}{2.f.p_{out}} \tag{2}$$

The secondary inductance L_s is taken from (2).

$$L_s = m^2 L_p \tag{3}$$

Thus, the total magnetic energy that has been stored is:

$$W = \frac{1}{2} L_p i_{in}^2 = \frac{1}{2} L_s \, i_{out}^2 = 3.125.10^{-9} J \tag{4}$$

The highest energy volume density is:

$$W_{vmax} = \frac{B_{max}^2}{2.\mu_{NiZn}} = 25.59 J/m^3 \tag{5}$$

The volume of the core is:

$$V = \frac{W}{W_{vmax}} = 1.22.10^{-10} m^3 \tag{6}$$

Thus, 0.122 mm3 of NiFe is required to store 3.125 nJ. We chose the square shape, Figure 3, for windings with outer diameter equal to 1500 µm and inner diameter equal to 750 µm. The core thickness is given by (7):

$$e_{NiZn} = \frac{V}{d_{out}^2} \tag{7}$$

2.5. Results of the geometrical and electrical sizing

Table 1 lists the main geometric and electrical parameters of the studied micro-coil. These parameters are used as input data for the electromagnetic and thermal simulations, carried out to analyze the behavior of the micro-coil and to optimize its operating performance. Due to the adaptation of mathematical models such as Maxwell's equations and the heat equation to simulate the magnetic, electric, and thermal phenomena, a set of simplifying assumptions has been introduced in order to reduce the complexity and the inherent mathematical nonlinearity. These assumptions are consistent with those commonly adopted in the literature [20] by researchers in this field.

- The isotropy of the various materials under investigation.
- The temperature affects the thermal conductivity coefficient.
- Thermal convection is introduced as a boundary condition for the substrate-microcoil assembly.

Table 1. Values of geometric and electrical parameters

Geometric parameters	Electrical parameters
d_{out}=1500µm, d_{in}=750µm, e=54.27 µm, ó=6.56 µm, n_p=5, n_s=2, w_p=46.39 µm, w_s=169.6 µm, t_p=13.13 µm,t_s=13.13 µm, s_p=35.75 µm, s_s=35.75 µm,l_p=2.25cm, l_{ts}=9mm	L_p=36nH, Rs_p=1.45 Ω, Rs_s=0.16 Ω, R_{magp}=103.98K Ω, R_{mags}=71.1K Ω, R_{subp}=3.54 K Ω, Ls=6.25Nh, R_{subs}=2.42K Ω, C_{oxp}=2.5Pf, C_{oxs}=3.66pF, C_{kp}=0.14 pF, C_k=10.79 pF, C_{subp}=0.54 pF, C_{subs}=0.79 pF, C_{ks}=0.057 pF.

The assumption of homogeneity and isotropy is based on the fundamental principles of material behavior. In general, the governing mathematical equations and models for physical phenomena, such as electromagnetic and thermal processes, are formulated under the assumption of homogeneous and isotropic materials, where the spatial variation of thermo physical and electrical properties is neglected. In the present study, applied to the micro planar transformer, the material properties are considered independent of both direction and position, which enables the direct application of the governing equations while simplifying the overall model. Furthermore, convective effects are neglected within the fluid mechanics framework, as the micrometric dimensions of the transformer ensure, based on the Rayleigh number estimation, that natural convection around the coils is negligible. Thus, air particle motion surrounding the coils is ignored, and convective heat transfer is only accounted for at the boundaries through Robin-type boundary conditions.

3. MICROTRANSFORMER MAGNETOTHERMAL BEHAVIOR

3.1. Mathematical model

The studied phenomenon is modeled by a set of coupled equations combining Maxwell's equations with the heat equation, following the geometrical design and sizing of the transformer. Dimensioning of the micro-coils of primary and secondary: the equations show that the primary and secondary inductances of the micro-transformer are directly connected to the energy stored. For a maximum current, that is to say for $t = \alpha T$, $W = \frac{1}{2} L_p i_{1max}^2 = \frac{1}{2} L_s i_{2max}^2$, $P = \frac{W}{T} = \frac{1}{2T} L_p I_{1max}^2$, $I_{1max} = \frac{V_e \alpha T}{L_p}$, $P = V_s I_s = \frac{V_e^2}{2L_p} \alpha^2 T$. The value of the primary inductance L_p of the micro-transformer is derived there from: $L_p = \frac{V_s^2 \alpha^2 T}{2 V_s I_s}$ and $m = \frac{\alpha}{(\alpha-1)} \frac{\mathrm{V_s}}{\mathrm{V_e}}$. With $\alpha = 0.5$ then m equals 0.42. $L_s$of the micro-transformer is $L_s = \mathrm{m^2 L_p}$.

The density of energy is given by (8):

$$W_{vmax} = \frac{B_{max}^2}{2.\mu_0 \mu_r} \quad (8)$$

3.1.1. Maxwell's equations

The electromagnetic phenomenon is governed by Maxwell's equations, the resolution of the latter will allow us to visualize the magnetic behavior of the micro transformer [20], $\nabla \mathrm{x} \vec{H} = \vec{\mathrm{J}}$, $\nabla \mathrm{x} \vec{A} = \vec{\mathrm{B}}$, $\vec{E} = -\vec{\nabla}\mathrm{V} - j\omega\vec{A}$, $\vec{J} = \sigma\vec{E} + j\omega\vec{D}$, $\nabla\vec{J} = 0$,$\vec{B} = \mu_0\mu_r\vec{H}$, $\vec{D} = \varepsilon_0\varepsilon_r\vec{E}$.

3.2. Physical model

Based on the initial specifications, the characteristics of the micro-converter are established, thus forming the starting point for the micro-transformer's design. The latter consists of two coils deposited on a magnetic material, separated by a dielectric layer that acts both as an electrical insulator and as a magnetic coupling support (Figure 5). Figure 6 illustrates the study area and its boundaries.

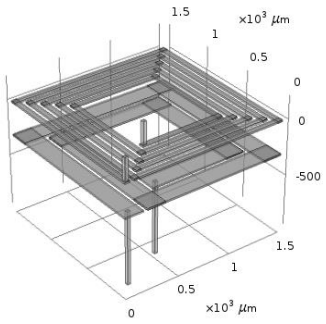

Figure 5. Physical model of a micro-planar transformer

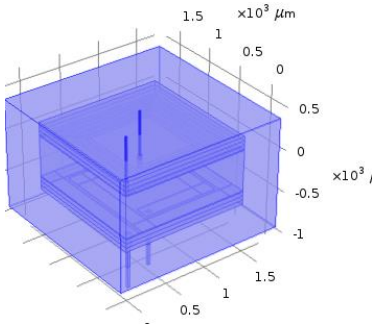

Figure 6. Domain boundaries study of the planar transformer

3.3. General conditions of simulation

Figure 6 displays the boundary conditions on the study domain's borders, which are:

$$\left(\vec{n}\vec{A}\right) = 0 \tag{9}$$

$$n_x A_x + n_y A_y + n_z A_z = 0 \tag{10}$$

$$\vec{n}.\vec{J} = 0 \tag{11}$$

Where: $\vec{n} = n_x\vec{\imath} + n_y\vec{\jmath} + n_z\vec{k}$is the normal vector to the boundary from where:

$$n_x.J_x + n_y.J_y + n_z.J_z = 0 \tag{12}$$

In our study domain, the simulation also needs initial conditions. Figures 7(a) and (b) present the current input and output, respectively.

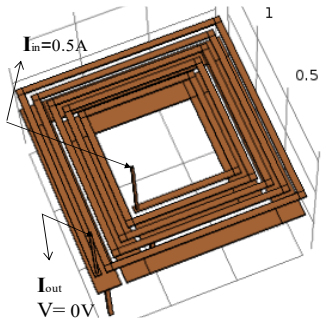

(a)

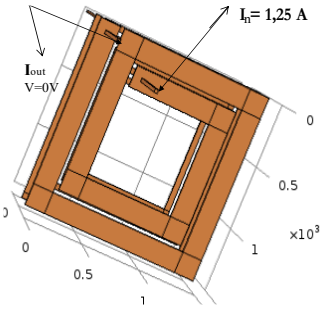

(b)

Figure 7. Initial operating conditions of the planar transformer: (a) input and output+ of the primary current and (b) input and output of the secondary current

3.4. Meshing of study domain

The COMSOL Multiphysics finite element method (FEM) was used for the numerical simulation, where the governing equations of the studied phenomenon have been discretized and transformed into a solvable algebraic system. A tetrahedral mesh has been selected due to the geometrical complexity of the domain; Figure 8, particularly the intricate coil structures of the transformer, which makes tetrahedral elements more suitable than structured meshes such as hexahedral ones. A rigorous mesh convergence test has been performed by progressively refining the mesh until the numerical results became independent of the element size, both in the magnetoelectric and thermal domains. The final mesh ensured an acceptable compromise between accuracy and computational cost, with the relative error constrained below 10-5.

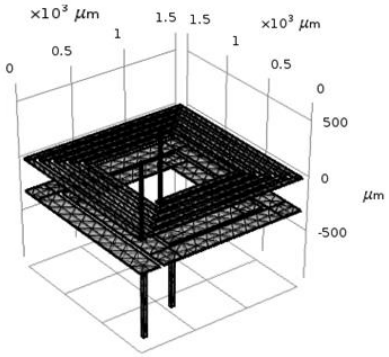

Figure 8. Mesh of micro-planar transformer

4. SIMULATION RESULTS AND DISCUSSION

4.1. Electric potential and magnetic field distribution

Figure 9 shows the distribution of electrical potential within the primary and secondary windings of the microtransformer. It can be seen that the potential reaches its maximum value at the current injection point and then gradually decreases along the spiral due to the intrinsic resistivity of the conductor. This decrease reflects the presence of a distributed ohmic resistance, responsible for energy dissipation through Joule heating. Thus, the regions where the voltage drop is more pronounced correspond to the areas of most significant power loss, reflecting the direct influence of the material's electrical properties on the overall behavior of the device.

Figure 10 show the distribution of the magnetic field within the micro-coil, and in the micro-transformer. It can be observed that the magnetic field intensity is highest at the center of the micro-coil, particularly along the inner boundaries of the windings, where the current density is more concentrated. This strong localization of the field is a direct consequence of the coil geometry and the proximity of the current-carrying conductors, which enhance the magnetic flux linkage in the central region. As the distance from the coil center increases toward the outer edges, the magnetic field gradually decreases due to flux dispersion in the surrounding medium. In the case of the complete micro-transformer, the superposition of fields generated by the primary and secondary windings leads to a more complex distribution, where regions of high field intensity are observed in the vicinity of both coils, while the field strength diminishes further away from the active magnetic region [20], [21].

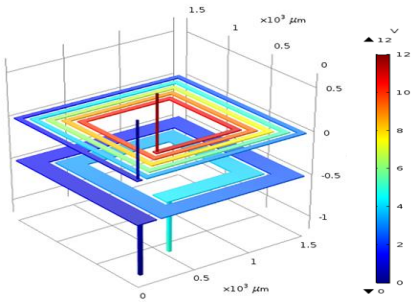

Figure 9. Potential distribution in the coils of the planar transformer

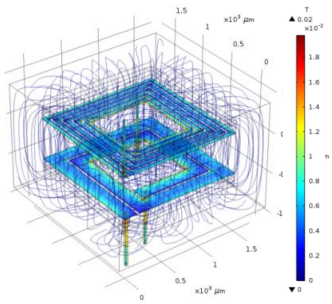

Figure 10. Magnetic field distribution in the micro-transformer

4.2. Current density distribution in the conductors

Solving Maxwell's equations [20] allows for a three-dimensional representation of the current density distribution within the microtransformer, thus providing a detailed understanding of the structure's electromagnetic behavior. Figures 11(a) and (b) illustrate the current density distribution in the primary and secondary windings of the device, respectively. It appears that the current density reaches a minimum value at the coil output, a phenomenon attributed to the intrinsic resistance of the conductive material. This distribution is non-uniform along the spiral: higher current concentrations are observed at the corners,

generating areas of locally increased resistance and therefore greater ohmic losses. These distribution irregularities are directly related to the geometry of the structure and the configuration of the conductive path. Furthermore, skin and proximity effects are clearly identifiable, manifesting more pronouncedly between adjacent turns. These electromagnetic phenomena contribute to an increase in Joule effect losses and significantly influence the overall performance of the microtransformer, particularly in terms of efficiency and thermal behavior.

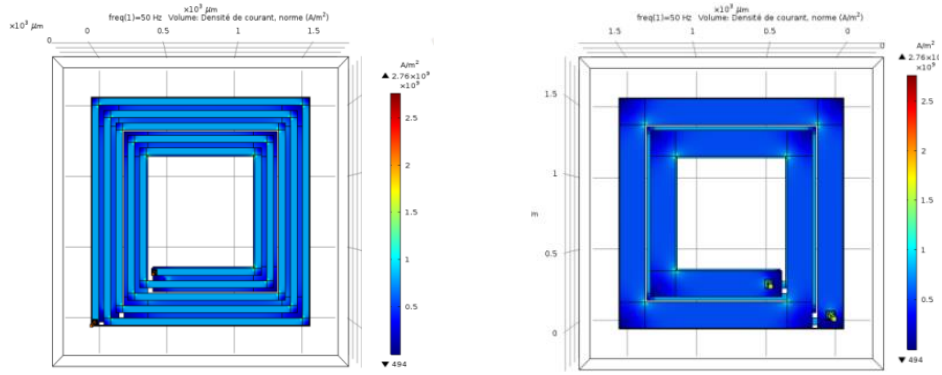

(a) (b)

Figure 11. Current distribution in the micro-transformer: (a) primary and (b) secondary

4.3. Magnetic field distribution vs the gap

Figure 12 shows the distribution of magnetic field lines within the microtransformer for different air gap values, corresponding to the space separating the two microcoils. For small air gap values, the field lines are mostly confined to the central magnetic region, thus ensuring optimal coupling between the primary and secondary windings. Conversely, as the air gap increases, a progressive dispersion of the field lines is observed, indicating greater magnetic leakage. This dispersion reduces the efficiency of the magnetic coupling and results in a significant decrease in the inductance of both windings.

Figure 13 illustrates this evolution by showing the variation of inductance as a function of the air gap for the primary and secondary coils. The results show that the inductance values are maximum when the air gap is small, a condition that favors the concentration of magnetic flux in the magnetic material. As the air gap widens, the proportion of flux escaping into the air increases, leading to a progressive reduction in inductance. This behavior highlights the direct dependence of the microtransformer's electromagnetic performance on the air gap geometry.

Finally, Figure 14 illustrates the overall physical model of the microtransformer, integrating the various electromagnetic and geometric components of the device. This model provides an essential basis for understanding the coupling between the coils and for optimizing the component's efficiency in microscopic power conversion applications.

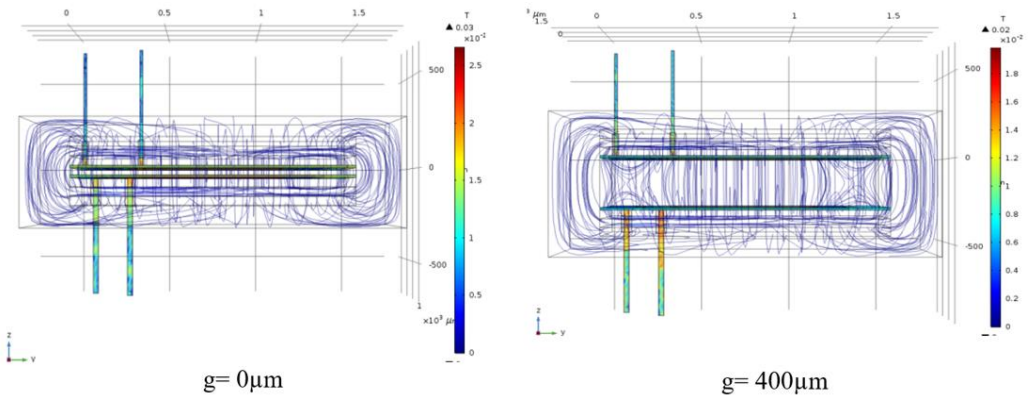

g= 0µm g= 400µm

Figure 12. Lines distribution magnetic field for different gaps

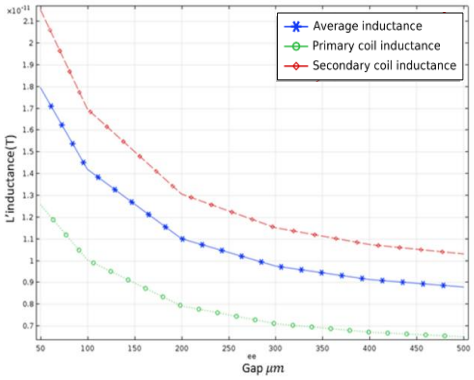

Figure 13. Variation of the inductance of the coil according to the gap

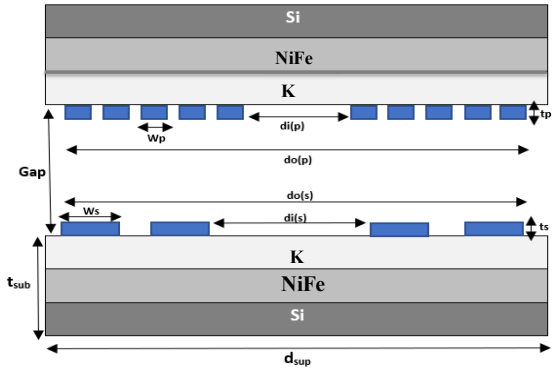

Figure 14. Longitudinal section of a micro-transformer

5. MICRO-TRANSFORMER THERMAL BEHAVIOUR

5.1. Physical model

For the study of the steady-state thermal behavior, we selected a model described by the heat equation in which the conductor is formed of conductors, the insulating layer is Kapton, the magnetic core is NiFe and the substrate is silicon, see Figure 14.

5.2. Mathematical model

Is used to calculate the temperature distribution in a specific area while accounting for the various transmission modes in (13) [22], [23].

$$\rho_i Cp_i \left[\frac{\partial T}{\partial t} + \vec{V}\nabla T\right] = \nabla(\lambda_i \nabla T) + p \tag{13}$$

p: source term if it is an internal heat generation. Each term of this equation has a physical meaning translating the thermal phenomenon into mathematical literature. The index i corresponds to the nature of the material: copper, printed circuit board (PCB) or air. The nature of the material is represented by the index I: copper, PCB, or air, temperature [K], air velocity (m/s) if in motion (convection), duration [s], source term that generates an internal heat flow [W/m3], material density [Kg/m3], material heat capacity [J/Kg.K], and material thermal conductivity [W/m.K]. Each term of this equation has a physical meaning translating the thermal phenomenon into mathematical literature. The following terms are used accumulative term which means the storage of heat during time, convective term (advective) if there is a movement of a self-supporting fluid, diffusive term (conductive) translates the way of propagation according to the nature of the material, source term if it is an internal generation of heat.

5.3. Simplification of the heat equation according to the considered assumptions

In this section, the general heat equation is simplified by taking into account the assumptions made for the microtransformer study. These assumptions mainly concern steady-state conditions, material homogeneity, and the geometric symmetry of the structure. They allow us to neglect certain conduction and convection terms, thus reducing the complete equation to a form more usable for the thermal analysis of the device. This simplification is an essential step in establishing a thermal model consistent with the actual operating conditions.

We can transcribe (23) in general writing, since our thermal study is conducted in three dimensions, by supposing:

$$\vec{V} = (\mathrm{u}, \mathrm{v}, \mathrm{w}) \text{ and } \lambda_i = \left(\lambda_{\mathrm{ix}}, \lambda_{\mathrm{iy}}, \lambda_{\mathrm{iz}}\right)\mathrm{I}$$

$$\rho Cp_i \left(\frac{\partial T}{\partial t} + u\frac{\partial T}{\partial x} + v\frac{\partial T}{\partial y} + w\frac{\partial T}{\partial z}\right) = \frac{\partial}{\partial \mathrm{x}}\left(\lambda_{\mathrm{ix}}\frac{\partial \mathrm{T}}{\partial \mathrm{x}}\right) + \frac{\partial}{\partial \mathrm{y}}\left(\lambda_{\mathrm{iy}}\frac{\partial \mathrm{T}}{\partial \mathrm{y}}\right) + \frac{\partial}{\partial \mathrm{z}}\left(\lambda_{\mathrm{iz}}\frac{\partial \mathrm{T}}{\partial \mathrm{z}}\right) + \mathrm{p} \tag{14}$$

– Negligible convection: $u = v = w = 0$

$$\rho_i Cp_i \frac{\partial T}{\partial t} = \frac{\partial}{\partial \mathrm{x}}\left(\lambda_{\mathrm{ix}}\frac{\partial \mathrm{T}}{\partial \mathrm{x}}\right) + \frac{\partial}{\partial \mathrm{y}}\left(\lambda_{\mathrm{iy}}\frac{\partial \mathrm{T}}{\partial \mathrm{y}}\right) + \frac{\partial}{\partial \mathrm{z}}\left(\lambda_{\mathrm{iz}}\frac{\partial \mathrm{T}}{\partial \mathrm{z}}\right) + \mathrm{p} \tag{15}$$

– Materials homogeneity

To $\lambda_{ix} = \lambda_{iy} = \lambda_{iz}$ and are constants,

$$\rho_i Cp_i \frac{\partial T}{\partial t} = \lambda_i \left(\frac{\partial^2 T}{\partial x^2} + \frac{\partial^2 T}{\partial y^2} + \frac{\partial^2 T}{\partial z^2}\right) + p \quad (16)$$

– In the stationary case

The source term represents the heat flux generated by the Joule effect in the conductor:

$$\lambda_i \left(\frac{\partial^2 T}{\partial x^2} + \frac{\partial^2 T}{\partial y^2} + \frac{\partial^2 T}{\partial z^2}\right) + p = 0 \quad (17)$$

Power lost by Joule loss:

$$P = RI^2 \quad (18)$$

By replacing the resistance formula:

$$P = \rho_0 \frac{L}{S_{moy}} I^2 \quad (19)$$

By expanding the source term:

$$p = \frac{P}{V} \quad (20)$$

v: conductor volume m^3

$$\mathrm{p} = \rho_0 \frac{\mathrm{L}}{\mathrm{VS_{moy}}} \mathrm{I}^2 \quad (21)$$

$$p = \rho_0 \frac{L}{S_{moy}\, L.S_{moy}} I^2 = \rho_0 \frac{I^2}{S_{moy}^2} \quad (22)$$

$$p = \rho_0 J^2 \quad (23)$$

The current density vector is:

$$\vec{J} = J_x \vec{\imath} + J_y \vec{\jmath} + J_z \vec{k} \left\|\vec{J}\right\|^2 = J^2 = J_x^2 + J_y^2 + J_z^2 \quad (24)$$

We replace it in (25):

$$p = \rho_0 \left(J_x^2 + J_y^2 + J_z^2\right) \quad (25)$$

Finally, our equation to solve is:

$$\lambda_i \left(\frac{\partial^2 T}{\partial x^2} + \frac{\partial^2 T}{\partial y^2} + \frac{\partial^2 T}{\partial z^2}\right) + \rho_0 \left(J_x^2 + J_y^2 + J_z^2\right) = 0 \quad (26)$$

5.4. General conditions of simulation and boundary conditions

The temperature and thermal convection imposed as conditions at the boundaries of the planar substrate-coil assembly determine the thermal conductivity coefficient and the isotropy of the various materials in the study domain. The term “micro-coil,” which is a heat source, is introduced in detail in (26). The coil, substrate, and air are all assumed to be at room temperature (20 °C) at time $t = 0$. A convective flow is supplied to the air box’s boundaries, given by (27) [24], [25]:

$$-\lambda_{air} \frac{\partial T}{\partial n}\rangle_{air\ border} = h_0 (T - T_\infty) \quad (27)$$

λ_{air}: air conductivity [W/m.°K], n: direction normal to the border [m], h_0: air convection coefficient [W/m2.°K], T_∞: ambient temperature.

5.5. Validation of the mathematical model

To verify the accuracy of our numerical results, we first compared one of our findings with those of earlier research by Benamer *et al*. [14] under identical simulation conditions (see Figure 15). The temperature distribution in the study area is shown below. Our model is validated by the apparent high degree of agreement between our results.

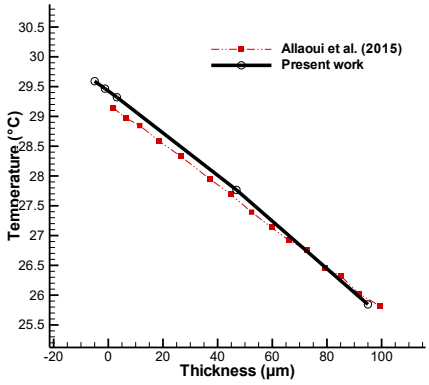

Figure 15. Temperature distribution in the core

6. SIMULATION RESULTS

6.1. Temperature distribution in micro transformer primary and secondary

6.1.1. In the le primary

Figures 16(a)-(d) illustrate the temperature distribution within the microtransformer. The temperature is highest in the microcoil conductors, which are the primary source of heat dissipation. As one moves away from the conductors, the temperature gradually decreases, stabilizing in the upper layers and reaching a maximum of approximately 40 °C at the spiral conductor. The Kapton region exhibits a relatively higher temperature due to its direct proximity to the microcoil conductor. The temperature gradient is more pronounced in Kapton than in the ferrite, which is explained by the lower thermal conductivity of Kapton compared to magnetic materials.

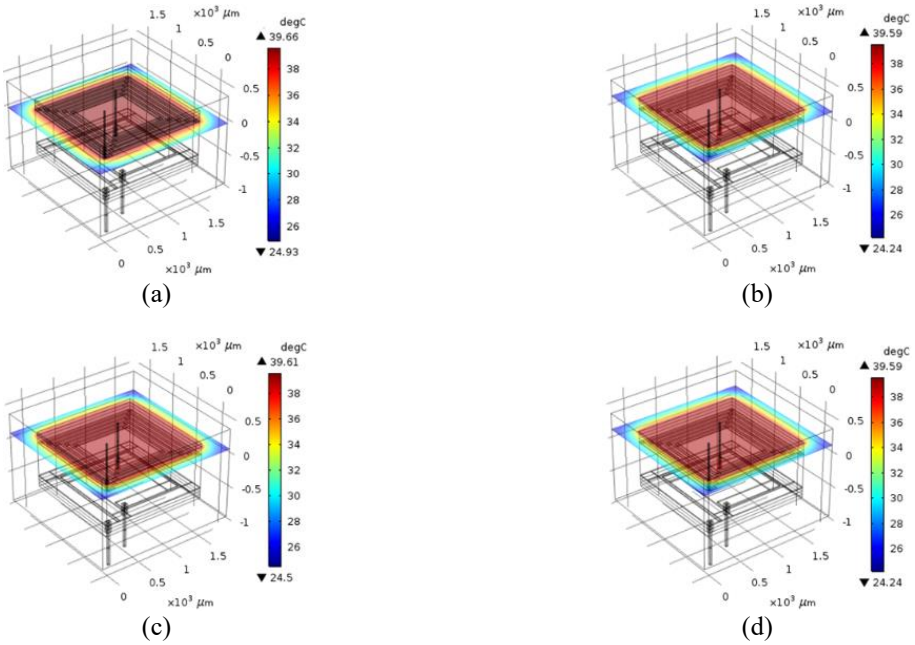

Figure 16. Temperature distribution in primary of micro-transformer: (a) conductor, (b) kapton$K$, (c) $N_i F_e$, and (d) silicon S_i

Furthermore, thermal convection plays a significant role in heat dissipation from areas not involved in heat generation, including the intercoil spaces, the dielectric insulation node (DIN) zone, and the substrate. It is important to note that the thermal conductivity coefficient acts inversely proportionally to the temperature gradient: the higher this coefficient, the weaker the gradient. Thus, the temperature decrease is more pronounced in insulators such as Kapton than in conductive materials like ferrite. Overall, the temperature field reaches its maximum in the immediate vicinity of the micro-coils, then gradually decreases as the distance from the active areas increases.

6.1.2. In the secondary

Figures 17(a)-(d)illustrate the spatial temperature distribution within the microtransformer. It is clear that the temperature reaches its maximum value at the microcoil conductors, which are the main sources of heat dissipation due to the ohmic losses generated by the flow of electric current. Figure 18 highlights a slight decrease in temperature between the coils, due to natural air convection. This cooling is even more pronounced inside the microcoil, where air circulation promotes more efficient dissipation of the heat accumulated in the conductors.

Furthermore, a significant temperature increase is observed at the vias, the areas where current flows between the different metallic layers. This localized overheating is explained by the high current density flowing through them, generating a greater heat flux than in the rest of the conductive tracks. The thermal behavior of the silicon layer differs markedly from that of the other materials constituting the structure. Due to its relatively high thermal conductivity, silicon acts as a natural heat sink, ensuring a homogeneous redistribution of heat across its surface. Thermal gradients are therefore very low, resulting in increased thermal stability.

Thus, the overall temperature distribution highlights the crucial role of materials and geometry in the thermal management of the microtransformer. Conductors and vias appear as critical areas of heat dissipation, while silicon plays a compensating role by promoting the thermal equilibrium of the entire device.

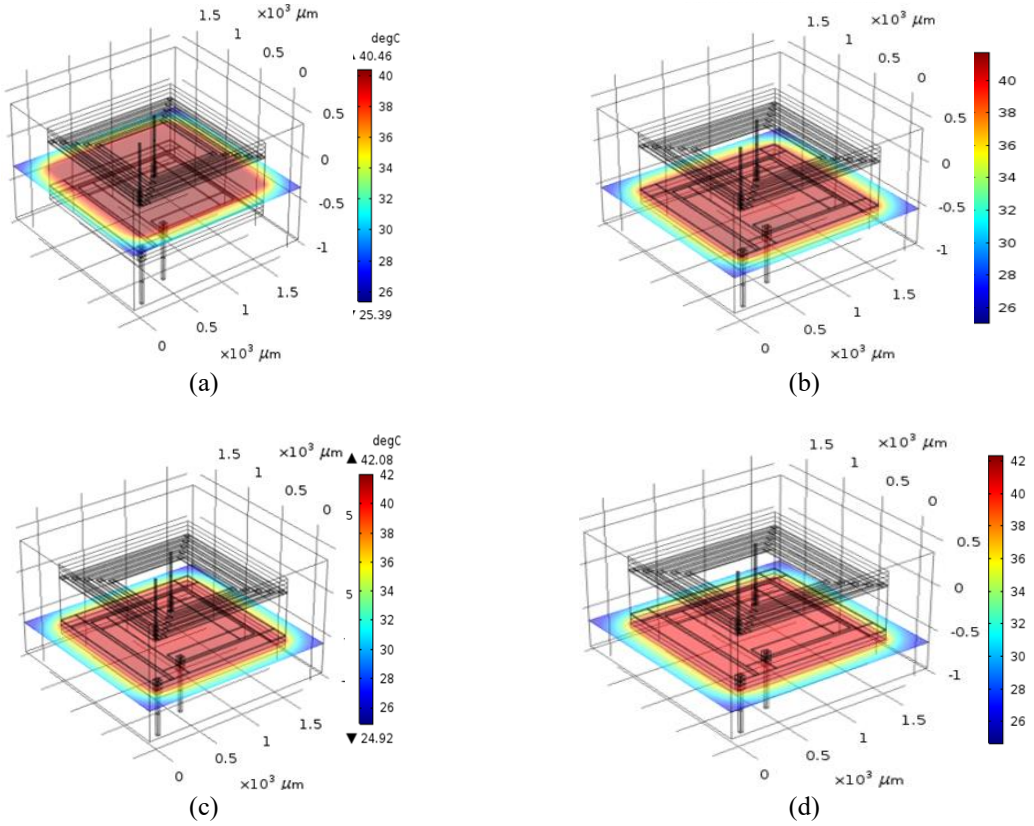

Figure 17. Temperature distribution in secondary of micro-transformer: (a) conductor, (b) kapton$K$, (c) $N_i F_e$, and (d) silicon S_i

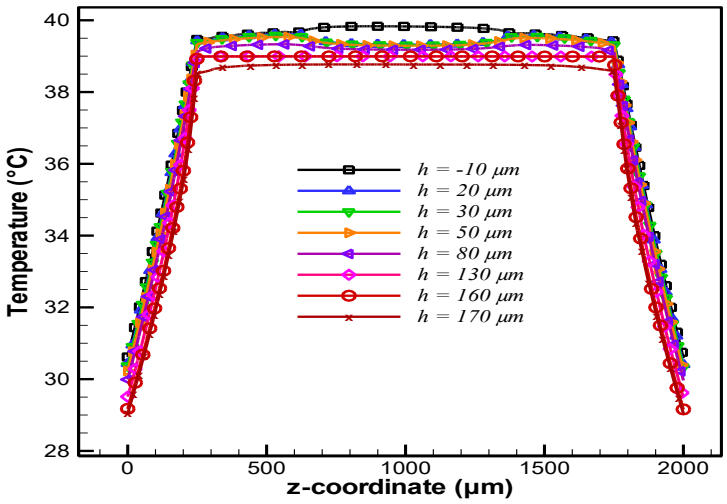

Figure18. Global graphs of the temperature slices

6.2. Temporal evolution of the temperature in the transformer primary and secondary

Figure 19 shows the time evolution of the average temperature within the different constituent parts of the microtransformer. As shown in Figure 19(a), the average temperature of the layers gradually increases over time, reflecting the transient heating phase of the device, until it reaches a steady state where the values stabilize between approximately 20 °C and 40 °C. This evolution demonstrates a thermal equilibrium established between the heat generated by Joule heating in the conductors and the dissipation to the outside by conduction and convection. Figure 19(b) provides a more detailed view of this evolution by showing an enlargement of the curve for each of the microtransformer layers. It appears that the average temperatures of the primary and secondary windings vary within two distinct ranges, a direct consequence of the presence of the air gap, which modifies the distribution of the heat flux and the heat exchange capacity between the two coils. The primary layer consistently exhibits the highest temperature, due to the higher current density flowing through it, resulting in greater ohmic losses and therefore increased heat dissipation. Conversely, the secondary layer, subjected to less electrical stress, experiences more moderate heating and reaches its steady state more quickly. This temperature difference between the two windings highlights the influence of magnetic coupling and the microtransformer's geometry on the overall thermal behavior of the device. Analyzing this time evolution is thus a crucial step in evaluating the thermal stability, reliability, and energy efficiency of the microtransformer under real-world operating conditions.

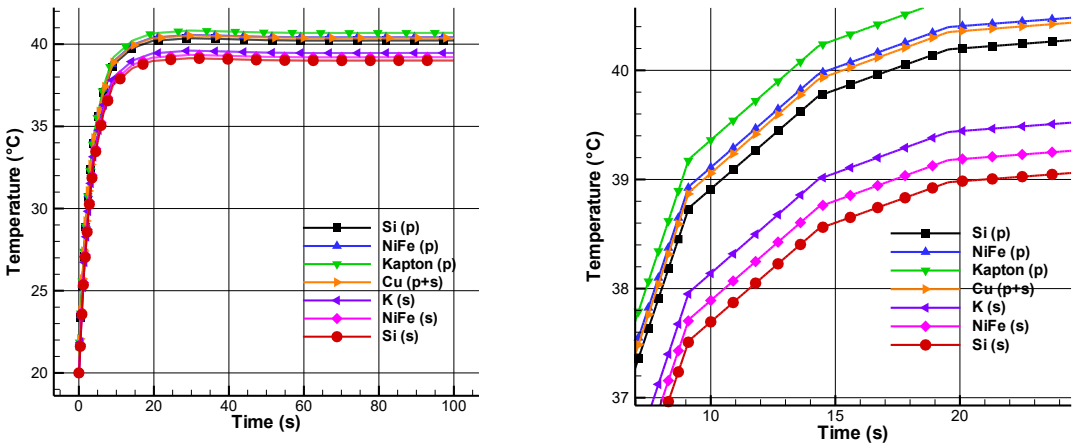

Figure 19. Temporal evolution of the average temperature in the different parts of the microtransformer: (a) in the primary (p) and secondary (s) areas and (b) zoom on the part between 0 and 20 seconds

7. CONCLUSION

The work presented in this paper focuses on the study of the magneto-thermal behaviour of a planar transformer over a very wide frequency range, intended for use in a flyback micro-converter. Planar transformers are increasingly used in low- and very low-power electronic devices because they offer major advantages in terms of size, efficiency and manufacturing. With a view to designing this structure, we conducted a study that enabled us to determine the various geometric and electrical parameters characterising our future transformer prototype. The study of magneto-thermal behaviour has revealed the distribution of currents and voltages, the magnetic field and the temperature distribution in the different layers of materials comprising the planar transformer. All of these results have made it possible to identify the optimal operation of the planar transformer. Future research will be conducted to expand the scope of application of this low-power transformer (LT) model to transformers for higher power ratings.

FUNDING INFORMATION

Authors state no funding involved.

AUTHOR CONTRIBUTIONS STATEMENT

This journal uses the Contributor Roles Taxonomy (CRediT) to recognize individual author contributions, reduce authorship disputes, and facilitate collaboration.

Name of Author	C	M	So	Va	Fo	I	R	D	O	E	Vi	Su	P	Fu
Tahar Alili	✓	✓	✓	✓	✓	✓	✓	✓	✓	✓			✓	
Fatima Zohra Medjaoui	✓	✓	✓			✓	✓	✓	✓	✓	✓	✓		✓
Azzedine Hamid	✓		✓	✓	✓	✓	✓	✓		✓	✓		✓	✓
Abderrahim Mokhefi	✓		✓				✓		✓			✓	✓	
Yacine Guettaf		✓	✓	✓	✓	✓	✓	✓		✓	✓		✓	
Hocine Guentri	✓	✓			✓		✓		✓			✓	✓	

C : **C**onceptualization
M : **M**ethodology
So : **So**ftware
Va : **Va**lidation
Fo : **Fo**rmal analysis
I : **I**nvestigation
R : **R**esources
D : **D**ata Curation
O : Writing -**O**riginal Draft
E : Writing - Review &**E**diting
Vi : **Vi**sualization
Su : **Su**pervision
P : **P**roject administration
Fu : **Fu**nding acquisition

CONFLICT OF INTEREST STATEMENT

Authors state no conflict of interest.

DATA AVAILABILITY

The authors declare that all data existing in this paper are available and can be made available to the publisher. Please contact T. A, the principal author of this paper.

REFERENCES

[1] M. A. Saket, M. Ordonez, and N. Shafiei, "Planar Transformers With Near-Zero Common-Mode Noise for Flyback and Forward Converters," *IEEE Transactions on Power Electronics*, vol. 33, no. 2, pp. 1554–1571, Feb. 2018, doi: 10.1109/tpel.2017.2679717.

[2] A. Abdeldjebbar, A. Hamid, Y. Guettaf, and R. Melati, "Design of micro-transformer in monolithic technology for high-frequency flyback-type converters," *Electrical Engineering*, vol. 100, no. 4, pp. 2589–2601, Jul. 2018, doi: 10.1007/s00202-018-0730-8.

[3] W. Water and J. Lu, "Performance comparison of integrated magnetics used in LLC resonant DC-DC converter for low voltage energy storage system," *2017 IEEE Innovative Smart Grid Technologies - Asia (ISGT-Asia)*, pp. 1–5, Dec. 2017, doi: 10.1109/isgt-asia.2017.8378344.

[4] M. A. Saket, N. Shafiei and M. Ordonez, "LLC converters with planar transformers: issues and mitigation," in *IEEE Transactions on Power Electronics*, vol. 32, no. 6, pp. 4524-4542, 2017, doi: 10.1109/TPEL.2016.2602360.

[5] V. C. Valchev and A. Van den Bossche, *Inductors and Transformers for Power Electronics*. CRC Press, 2018, doi: 10.1201/9781420027280.

[6] B. Li, Q. Li, and F. C. Lee, "High-Frequency PCB Winding Transformer With Integrated Inductors for a Bi-Directional Resonant Converter," *IEEE Transactions on Power Electronics*, vol. 34, no. 7, pp. 6123–6135, Jul. 2019, doi: 10.1109/tpel.2018.2874806.

[7] Z. Ouyang, O. C. Thomsen, and M. A. E. Andersen, "Optimal design and tradeoff analysis of planar transformer in high-power DC–DC converters," in *IEEE Transactions on Industrial Electronics*, vol. 59, no. 7, pp. 2800-2810, July 2012, doi: 10.1109/TIE.2010.2046005.
[8] M. Mu, L. Xue, D. Boroyevich, B. Hughes, and P. Mattavelli, "Design of integrated transformer and inductor for high frequency dual active bridge GaN Charger for PHEV," *2015 IEEE Applied Power Electronics Conference and Exposition (APEC)*, pp. 579–585, Mar. 2015, doi: 10.1109/apec.2015.7104407.
[9] T. Orosz, "Evolution and Modern Approaches of the Power Transformer Cost Optimization Methods," *Periodica Polytechnica Electrical Engineering and Computer Science*, vol. 63, no. 1, pp. 37–50, Jan. 2019, doi: 10.3311/ppee.13000.
[10] Y.-C. Liu *et al*., "Design and Implementation of a Planar Transformer With Fractional Turns for High Power Density LLC Resonant Converters," *IEEE Transactions on Power Electronics*, vol. 36, no. 5, pp. 5191–5203, May 2021, doi: 10.1109/tpel.2020.3029001.
[11] Z. Song and B. Zhou, "Miniaturized lumped quadrature hybrid using inductance- and integration-enhanced inductors for VHF band applications," *International Journal of RF and Microwave Computer-Aided Engineering*, vol. 32, no. 12, Sep. 2022, doi: 10.1002/mmce.23431.
[12] C. Pacurar et al., "High Frequency Analysis and Optimization of Planar Spiral Inductors Used in Microelectronic Circuits," *Electronics*, vol. 10, no. 23, p. 2897, Nov. 2021, doi: 10.3390/electronics10232897.
[13] M. I. Hassan, N. Keshmiri, A. D. Callegaro, M. F. Cruz, M. Narimani, and A. Emadi, "Design Optimization Methodology for Planar Transformers for More Electric Aircraft," *IEEE Open Journal of the Industrial Electronics Society*, vol. 2, pp. 568–583, 2021, doi: 10.1109/ojies.2021.3124732.
[14] K. Benamer, A. Hamid, E. Rossi di Schio, A. Mokhefi, R. Melati, and P. Valdiserri, "Magnetic and Thermal Behavior of a Planar Toroidal Transformer," *Energies*, vol. 17, no. 11, p. 2454, May 2024, doi: 10.3390/en17112454.
[15] H. Fisher *et al*., "Thermomechanical data of polyurethane shape memory polymer: Considering varying compositions," *Data in Brief*, vol. 32, p. 106294, Oct. 2020, doi: 10.1016/j.dib.2020.106294.
[16] A. Meshkat, R. Dehghani, H. Farzanehfard and S. A. Khajehoddin, "Improved On-Chip Inductor Design for Fully Integrated Voltage Regulators," in *IEEE Journal of Emerging and Selected Topics in Power Electronics*, vol. 10, no. 6, pp. 7397-7409, Dec. 2022, doi: 10.1109/JESTPE.2022.3199692.
[17] J.-S. N. T. Magambo, "Modeling and design of planar transformers for embedded DC/DC power converter," *HAL Theses*, Centrale Lille, France, 2017.
[18] J. S. N. T. Magambo *et al*., "Planar Magnetic Components in More Electric Aircraft: Review of Technology and Key Parameters for DC–DC Power Electronic Converter," *IEEE Transactions on Transportation Electrification*, vol. 3, no. 4, pp. 831–842, Dec. 2017, doi: 10.1109/tte.2017.2686327.
[19] X. Xiao *et al*., "Shape memory polymers with high and low temperature resistant properties," *Scientific Reports*, vol. 5, no. 1, Sep. 2015, doi: 10.1038/srep14137
[20] L. Pniak *et al*., "Planar Transformers Electromagnetic Modeling Considering Capacitive Couplings up to 100 MHz," in *IEEE Transactions on Power Electronics*, vol. 39, no. 6, pp. 7290-7301, 2024, doi: 10.1109/TPEL.2024.3365575.
[21] C. Østergaard, C. S. Kjeldsen, and M. Nymand, "Calculation of planar transformer capacitance based on the applied terminal voltages," *2020 IEEE 21st Workshop on Control and Modeling for Power Electronics (COMPEL)*, Aalborg, Denmark, 2020, pp. 1-7, doi: 10.1109/COMPEL49091.2020.9265797.
[22] R. Bakri, G. Corgne and X. Margueron, "Thermal Modeling of Planar Magnetics: Fundamentals, Review and Key Points," in *IEEE Access*, vol. 11, pp. 41654-41679, 2023, doi: 10.1109/ACCESS.2023.3269662.
[23] F. Khan, H. Hussein and M. I. Younis, "Spring-Shaped Inductor Tuned With a Microelectromechanical Electrothermal Actuator," in *IEEE Magnetics Letters*, vol. 11, pp. 1-5, 2020, doi: 10.1109/LMAG.2020.2982108.
[24] Z. Shen, Y. Shen, and H. Wang, "Thermal Modelling of Planar Transformers Considering Internal Power Loss Distribution," *2019 IEEE 4th International Future Energy Electronics Conference (IFEEC)*, pp. 1–5, Nov. 2019, doi: 10.1109/ifeec47410.2019.9015030.
[25] K. Gorecki and K. Gorski, "Compact thermal model of planar transformers," *2017 MIXDES - 24th International Conference Mixed Design of Integrated Circuits and Systems*, pp. 345–350, Jun. 2017, doi: 10.23919/mixdes.2017.8005229.

BIOGRAPHIES OF AUTHORS

Tahar Alili he obtained his Engineering degree in Electrical Engineering from the University of Science and Technology of Oran, USTO-MB (Algeria), in 1985, followed by his Master's degree in Insulating Materials and his Ph.D. in Electrical Discharges, both from USTO-MB, in 2010 and 2017 respectively. He is currently a lecturer and research laboratory member in the Department of Electrotechnics at USTO-MB. His research focuses on the integration of passive components for low-power electronics and renewable energies. He can be contacted at email: alili10@yahoo.fr.

Fatima Zohra Medjaoui she obtained her engineering degree in Electrical Engineering from the University of Science and Technology of Oran, USTO-MB (Algeria) in 1990, followed by her Master's degree in Insulating Materials and her Ph.D. in Passive Component Integration, both from USTO-MB, in 2006 and 2019 respectively. She is currently a lecturer and a member of the Integration for Power Electronics and Materials team within the Applied Power Electronics Laboratory in the Department of Electrical Engineering at USTO-MB. Her research focuses on the integration of passive components for low-power electronics and renewable energy applications. She can be contacted at email: fatimazohra.medjaoui@univ-usto.dz.

Azzedine Hamid he obtained his Engineering degree in Electrical Engineering from the University of Science and Technology of Oran, USTO-MB (Algeria) in 1987, followed by his Master's degree in Insulating Materials and his Ph.D. in Electrical Discharges, both from USTO-MB, in 1994 and 2005 respectively. He is currently a lecturer and head of the Integration for Power Electronics and Materials team within the Applied Power Electronics Laboratory in the Department of Electrical Engineering at USTO-MB. His research focuses on the integration of passive components for low-power electronics and renewable energy application. He can be contacted at email: a.hamid@cu-elbayadh.dz.

Abderrahim Mokhefi he obtained his Bachelor's degree in 2014, a Master's degree in Mechanical Engineering for Hydrocarbon Transport at M'Hamed BOUGARA University of Boumerdès, Algeria, and his Doctorate in Mechanical Engineering for Energy in 2016 and 2022 respectively. He is currently a teacher in fluid mechanics and renewable energies and is part of a research laboratory in mechanical engineering. He can be contacted at email: abderahimmokhefi@yahoo.fr.

Yacine Guettaf he obtained his Engineering degree in Electrical Engineering from the University of Tiaret (Algeria) in 2006, followed by his Master's degree in Insulating Materials and his Ph.D. in Electrical Discharges, both from USTO-MB, in 2012 and 2016 respectively. He is currently a member of the Integration for Power Electronics and Materials team within the Applied Power Electronics Laboratory in the Department of Electrical Engineering at University Center of el Bayadh. His research focuses on the integration of passive components for low-power electronics and renewable energy applications. He can be contacted at email: y_guettaf@yahoo.fr.

Hocine Guentri in 1996, he graduated from the Department of Electrotechnics of the Faculty of Electrical Engineering at the University Ibn Khaldun in Algeria. The Master's degree from the University of Saida Algeria. The Ph.D. degree from the University of Sidi Bel-Abbes, Algeria, in 2018.His research activities primarily concentrate on power systems, FACTS, renewable energy, and sustainable energy, and his research activities focus on smart grid systems and storage hybrid systems. He is a lecturer at the university centre Nour Bachir El Bayadh in Algeria. He can be contacted at email: h.guentri@cu-elbayadh.dz.